IEEE Journal of Microwaves

Received 20 September 2022; revised 16 November 2022 and 9 December 2022; accepted 12 December 2022. Date of publication 27 December 2022; date of current version 7 April 2023.

Digital Object Identifier 10.1109/JMW.2022.3229496

Modular Design of Waveguide Bandpass Filters With Improved Stopband and High Selectivity

ZAI-CHENG GUO [1], LONGJI CHEN[1], AND LEI ZHU [2] (Fellow, IEEE)

(Regular Paper)

[1]School of Electrical and Automation Engineering, Nanjing Normal University, Nanjing 210046, China
[2]Department of Electrical and Computer Engineering, Faculty of Science and Technology, University of Macau, Macau SAR 999078, China

CORRESPONDING AUTHOR: Zai-Cheng Guo (e-mail: yb67454@umac.mo).

This work was supported in part by the National Natural Science Foundation of China under Grant 62101272, in part by the Natural Science Foundation of Jiangsu Province under Grant BK20200726, and in part by the State Key Laboratory of Milli-Meter Waves under Grant K202120.
This work did not involve human subjects or animals in its research.

ABSTRACT A class of waveguide bandpass filters (BPFs) with parallel coupling topology is proposed by stacking rectangular cavities. Compared with transversal filters, each layer comprises more than one cavity, and these cavities are cascaded with electric or magnetic coupling. The stopband performance could be improved by properly adjusting the width-length ratio of rectangular cavity to push up the higher-order modes in the cavities, while the attractive property of transversal filter, i.e., modular design, is still valid and useful in simplifying the filter design process and producing transmission zeros (TZs) out of the passband. A fourth -, sixth -, and seventh-order BPF is successively designed, and frequency of the first spurious mode is increased from 1.12 to 1.48 times the operating frequency. Due to the parallel coupling topology, multiple TZs are generated at both sides of the passband, making the suppression more than 20 dB out of passband. Among these filters, the fourth- and sixth-order BPFs are fabricated, and the measured results demonstrate the effectiveness of the proposed method.

INDEX TERMS Capacitive iris, modularity, rectangular waveguide, stopband performance, transmission zero (TZ).

I. INTRODUCTION

Modern communication system has an urgent requirement for bandpass filters (BPFs) with high selectivity, low insertion loss, wide stopband and compact size. Waveguide filters are widely used because of their advantages in power capability and quality factor (Q). Recently, a modular method is proposed to design waveguide filters based on the transversal topology [1], [2], which enables a high-order filter to be divided into several sub-filters and each sub-filter could be separately realized. As a result, the complexity of designing high-order filters could be reduced. However, one drawback of these transversal filters is that the spurious passband caused by the higher-order modes is close to the working passband, which will impose re-strictions on some applications.

In the past decades, a variety of approaches have been proposed to suppress the spurious passbands [3]. In the early stages, a low-pass filter is cascaded to improve stop-band performance [4], [5], which is effective, but greatly increases the volume of the entire filter. In [6] and [7], by modifying the width of each resonator, the spurious responses are pushed up in frequency, while the basic resonance remains unchanged. In [3], [8] and [9], stepped impedance resonators are introduced to control the second resonant frequency by adjusting the length and impedance ratio of each resonator. The above two methods successfully push the spurious resonance up to 1.5 times the center frequency or more, but require higher manufacturing costs. In [10], an improved structure using capacity-loaded resonators is proposed to suppress the parasitic passband to 4 times the center frequency. In [11], by adjusting the placement of the coupling irises, the propagation of higher-order modes can be weakened, which makes it difficult to form parasitic passbands. In [12] and [13], metal

inserts placed in the E-plane of a rectangular waveguide along the waveguide axis can have the effect of broadening the stopband. In [14] and [15], rectangular slots are etched to suppress the second mode and reduce the coupling of the third mode.

To improve the stopband performance while preserving the modularity of filters in [1], [2], a new coupling topology was proposed in [16], where there were multiple parallel coupling paths between the input and output ports, and more than one resonator was included in each coupling path. This paper is a substantial extension of the work in [16], where the detailed design process, measured results and extension to higher-order filter, are presented in this paper. To realize the parallel coupling paths between input and output ports, the stacked configuration in [1], [2], is used, leading to a multi-layer configuration, where each layer could implement each sub-filter separately. However, different from the work in [1], [2], each layer no longer contains only one cavity in this paper, which makes the arrangement of the cavities of coupled resonator filters more flexible. On the other side, capacitive and inductive irises, instead of odd and even modes [1], are employed to realize the required positive/negative couplings, which means there will be less spurious interference nearby the passband. Therefore, the stopband range could be enlarged by properly setting the width-length ratio of rectangular cavities, while the desired transmission zeros (TZs) out of the passband are preserved, due to the multiple parallel coupling paths between input and output ports.

The remainder of this paper is arranged as follows. Section II presents the method to improve stopband performance. Next, a fourth-order BPF is designed in detail as an example to illustrate the design process. Afterward, two additional higher-order BPFs are presented by applying the process to further verify the method in Section IV. Section V draws the conclusion.

II. THE METHOD OF IMPROVING STOPBAND

To achieve a wide stopband above the passband, frequencies of the first few modes in a rectangular cavity will be studied first. As the heights of the cavities utilized are generally thin, the excited modes are TE_{m0n} modes, and their frequencies are given in (1).

$$f_{m0n} = \frac{v_0}{2\pi}\sqrt{\left(\frac{m\pi}{a}\right)^2 + \left(\frac{n\pi}{c}\right)^2} \tag{1}$$

where v_0 is the speed of light in free space; m, and n are half-wavelength numbers along X and Z axis, respectively; a, b, c are the width, height and length of a rectangular waveguide cavity, respectively.

The electric field distribution of the first four modes in the cavity is shown in Fig. 1. In these designs, the filters are all symmetric along the X-Y and Z-Y planes, and the input and output ports are placed in the center of the wide side, so the TE_{201} mode will not be excited. Therefore, the first few modes to be taken into consideration are TE_{101}, TE_{102}, and TE_{301} mode. Based on the formula in (1), the relationship between

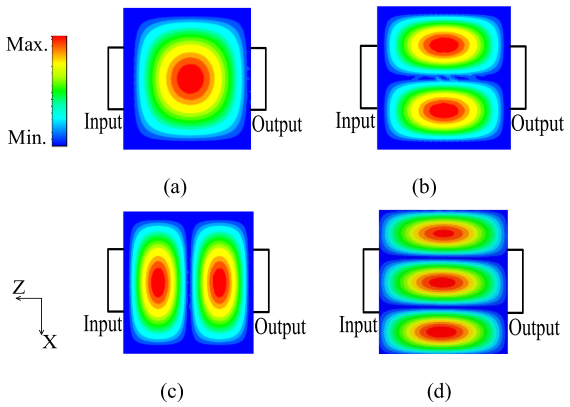

FIGURE 1. Electric field distribution of the first four modes in a thin cavity.

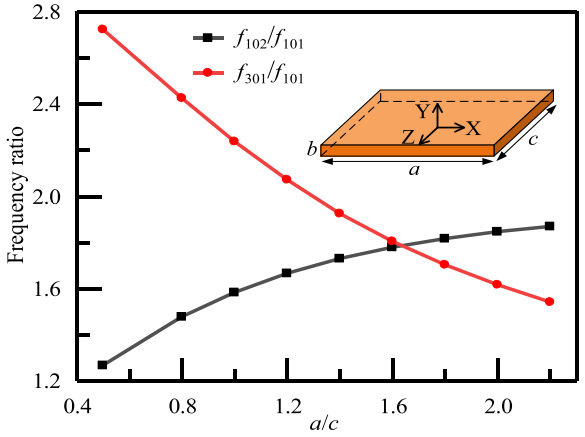

FIGURE 2. Frequency ratio of different modes versus the width-length ratio of a rectangular cavity.

the frequency ratio of these modes and the width-length ratio (a/c) of a rectangular cavity is given in Fig. 2. As the fundamental mode TE_{101} is the desired mode used to design filters, then the spurious modes need to be pushed up as far away from the operating frequency as possible, which means the frequency ratio should be as large as possible.

In this case, the values of f_{102}/f_{101} and f_{301}/f_{102} should be taken into consideration for the interference of higher-order modes. As can be obtained from Fig. 2, when the width-length ratio is 1.63, the two frequency ratios, f_{102}/f_{101} and f_{301}/f_{102}, are equal, thus achieving a maximum of 1.78, which means the widest stopband is about $1.78f_0$. Otherwise, either TE_{102} or TE_{301} mode will appear before $1.78f_0$.

After determining the working frequency and the most appropriate value of the width-length ratio, the initial width and length of the cavities could be obtained using formula (1) once the working frequency of filter is given.

III. IMPLEMENTATION OF A FOURTH-ORDER BPF

In this section, the filter design procedures will be described in detail through a fourth-order cavity BPF, and then the simulated and measured results will be presented to verify

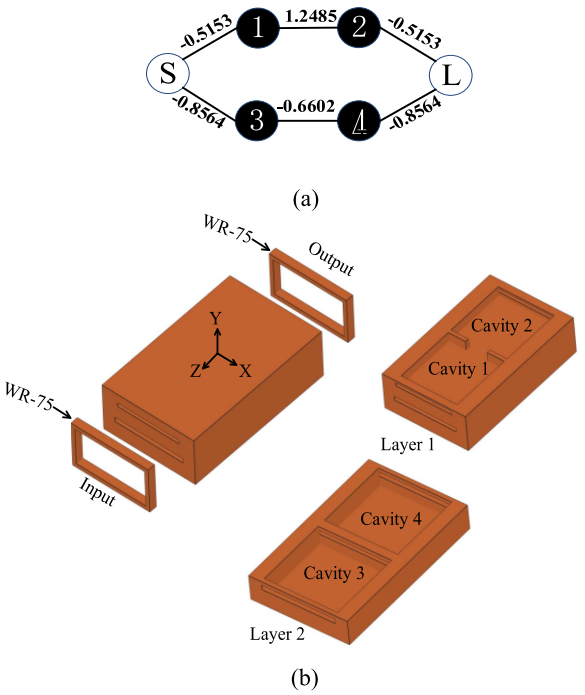

FIGURE 3. (a) Topology of the proposed fourth-order BPF; (b) Configuration of the proposed fourth-order BPF.

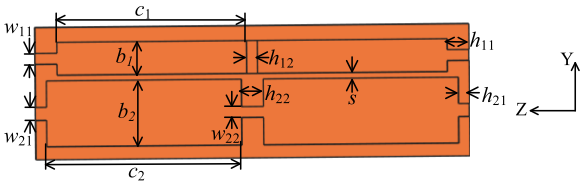

FIGURE 4. The side sectional view of the proposed fourth-order BPF.

the proposed approach. All simulated filtering responses are performed in the EM simulator CST.

The specification of the fourth-order BPF is given as follows: working frequency $f_0 = 12$ GHz, bandwidth $BW = 400$ MHz, in-band return loss RL ≥ 20 dB, and two TZs are set at 11.6 GHz and 12.4 GHz, respectively. To achieve the specification, the topology in Fig. 3(a) is applied.

According to the topology, it could be seen there are two parallel paths between the input and output ports. The first path includes the first and second resonator, i.e., R_1 and R_2, and the second path includes the third and fourth resonator, i.e., R_3 and R_4. The configuration in Fig. 3(b) is used to realize the filter. The whole structure is symmetric along the X-Y and Z-Y planes. Two stacked layers are connected to the input/output port in parallel. Each layer comprises two cascaded cavities, and each cavity contributes one waveguide resonator. As shown in Fig. 3(b), the two cavities in Layer 1 are called cavity 1 and cavity 2, and the two cavities in Layer 2 are called cavity 3 and cavity 4. The cavities in the same layer are with the same size. As the subgraph of Figs. 2 and 4 describe, the width of cavity 1 and cavity 2 is a_1, and the height and length

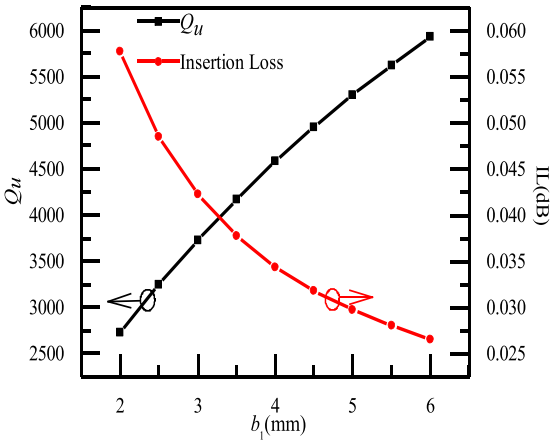

FIGURE 5. Variation of Q_u and insertion loss with respect to the cavity height b_1.

are b_1 and c_1, respectively. The width of cavity 3 and cavity 4 is a_2, and their height and length are b_2 and c_2, respectively. The distance between the two layers is denoted s. On both sides of the entire filter, standard waveguide WR-75 is used as input and output port. The input/output port and the cavities, as well as the cavities of the same layer, are connected by coupling irises.

Since how to set the initial values of a and c of a cavity have been discussed in the previous section, the following sections will cover several other critical parameters of the sub-filters.

A. UNLOADED QUALITY FACTOR AND INSERTION LOSS

For TE_{101} mode, the height b of a rectangular cavity mainly affects the unloaded quality factor (Q_u) of the resonant cavity while the width and length determine the resonant frequency. In this section, let's take the height b_1 of Layer 1 as an example. In the EM simulator CST, the trend of variation of Q_u with respect to the cavity height b_1 can be extracted, as shown in Fig. 5. It can be seen from the figure that when the cavity height increases from 2 mm to 6 mm, the Q_u of the cavity increases from 2730 to 5930. Simultaneously, given a Q_u of the resonator, the insertion loss (IL) can be estimated [17], and the result is also shown in Fig. 5. As the two layers are connected in parallel to the input/output port, the cavity height in each layer will be constrained by the height of the feeding waveguide WR-75. Therefore, the choice of height for each layer needs a comprehensive consideration. In this design, the heights of Layer 1 and Layer 2 are finally set at 6 mm, and the selection of these two parameters has a certain degree of freedom. Correspondingly, Q_u of the cavities in Layer 1 and Layer 2 are determined as the value of 5930.

B. EXTERNAL QUALITY FACTORS (Q_e)

The coupling strength between the input/output port and the cavities is indicated by Q_e, which can be extracted according to the process in [17]. The main parameters influencing Q_e are the size and thickness of the coupling iris in the corresponding position. Note that in the coupling topology, the coupling

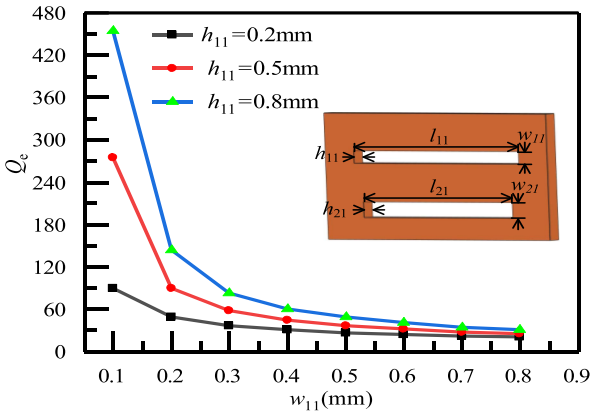

FIGURE 6. Variation of Q_e with respect to the width w_{11} and thickness h_{11} of the coupling iris.

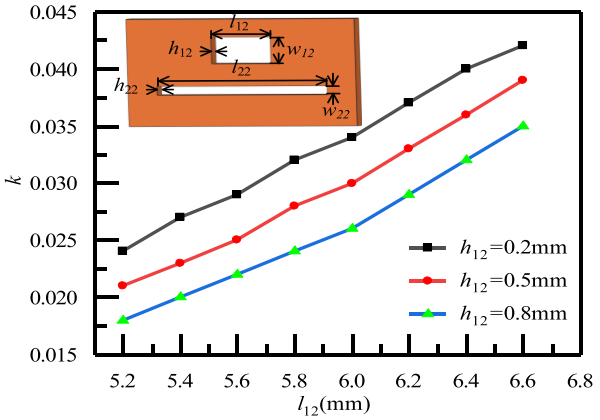

FIGURE 7. Variation of inter-cavity coupling coefficient with respect to the length l_{12} and thickness h_{12} of the coupling iris.

coefficient corresponding to this position is negative, and thus the capacitive iris is introduced [18], [19], [20]. As shown in Fig. 4, and in the subgraph of Fig. 6, the length of the capacitive iris is labeled as l_{11}, which is equal to the cavity length a_1, while the width and thickness are labeled as w_{11} and h_{11}, respectively, which are the two degrees of freedom that could affect Q_e. Fig. 6 shows the variation of the extracted Q_e with respect to width w_{11} and thickness h_{11}. When h_{11} is constant, the larger w_{11}, the smaller Q_e; when w_{11} is constant, the larger h_{11}, the larger Q_e. As the width and thickness both could be used to adjust Q_e, the thickness of the coupling iris is used as a parameter for adjustment to maintain the whole length in each layer equal.

C. INTER-CAVITY COUPLINGS

The coupling coefficient between the inner cavities could be extracted. In the case of cavity 1 and cavity 2, the coupling coefficient between them is positive, so the inductive iris is used. The width of the coupling iris is labeled as w_{12}, which is equal to the height of the cavities, and the length and thickness are labeled as l_{12} and h_{12}, respectively. The variation of inter-cavity coupling coefficient with respect to the length l_{12} and thickness h_{12} of the coupling iris is shown in Fig. 7. As seen from the figure, larger l_{12} or smaller h_{12} could both achieve the larger coupling coefficient. Although the coupling coefficient between cavity 3 and cavity 4 is negative, the extracting solution is similar.

According to the above procedures, the initial parameters of the filter can be determined. In the configuration shown in Fig. 3(b), there is no coupling relations between the two paths, which means that each layer can be designed and adjusted independently without affecting the other. In other words, the proposed fourth-order BPF could be divided into two second-order sub-filters and realize them separately [1], [2]. Guided by this idea, the overall response is decomposed and the structure of waveguide cavities in each layer is adjusted separately and finely to match the ideal matrix. The comparison between the simulated results and matrix of each sub-filter is shown in Fig. 8. It could be seen that the simulated results of each

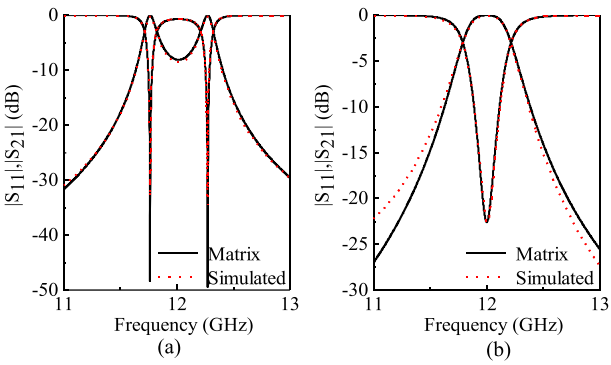

FIGURE 8. Comparison between simulated results and matrix of each sub-filter of the fourth-order BPF, (a) sub-filter 1, (b) sub-filter 2.

sub-filter are in good agreement with the filtering response of the coupling matrix near the operating frequency. Due to the presence of spurious modes in the lower and upper stopband, there are some discrepancies at both sides of the passband.

By combining the two sub-filters, the final filtering response could be obtained after fine tuning in the EM simulator. The final values of all parameters are: $a_1 = 18.65$ mm, $a_2 = 18.47$ mm, $b_1 = 6$ mm, $b_2 = 6$ mm, $c_1 = 16.3$ mm, $c_2 = 19.5$ mm, $h_{11} = 3.7$ mm, $h_{21} = 0.5$ mm, $h_{12} = 2$ mm, $h_{22} = 2$ mm, $l_{11} = 18.65$ mm, $l_{12} = 7.7$ mm, $l_{21} = 18.47$ mm, $l_{22} = 18.47$ mm, $s = 0.4$ mm, $w_{11} = 1.02$ mm, $w_{12} = 6$ mm, $w_{21} = 0.71$ mm, $w_{22} = 0.255$ mm. Finally, the prototype filter is fabricated with silver-plated copper through CNC milling process, and assembled by screws. The photograph of the fabricated BPF is shown in Fig. 9. The simulated and measured results, as well as coupling matrix's responses, are displayed in Fig. 10(a). It can be seen the simulated results in passband agree well with the matrix in terms of operating frequency, bandwidth, return loss and zero position. On the left side of the passband, some differences occur due to the influence of the spurious modes in the lower passband. As for the measured results, the center frequency is about 11.97 GHz, which is slightly offset. In terms of insertion loss, the simulated and measured results are approximately 0.24 dB

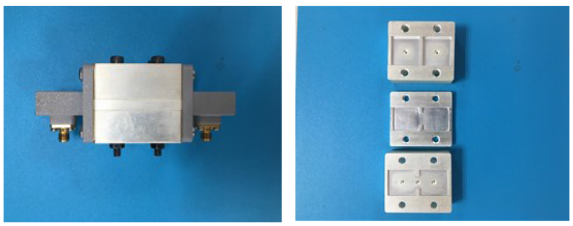

FIGURE 9. Photograph of the fabricated fourth-order BPF.

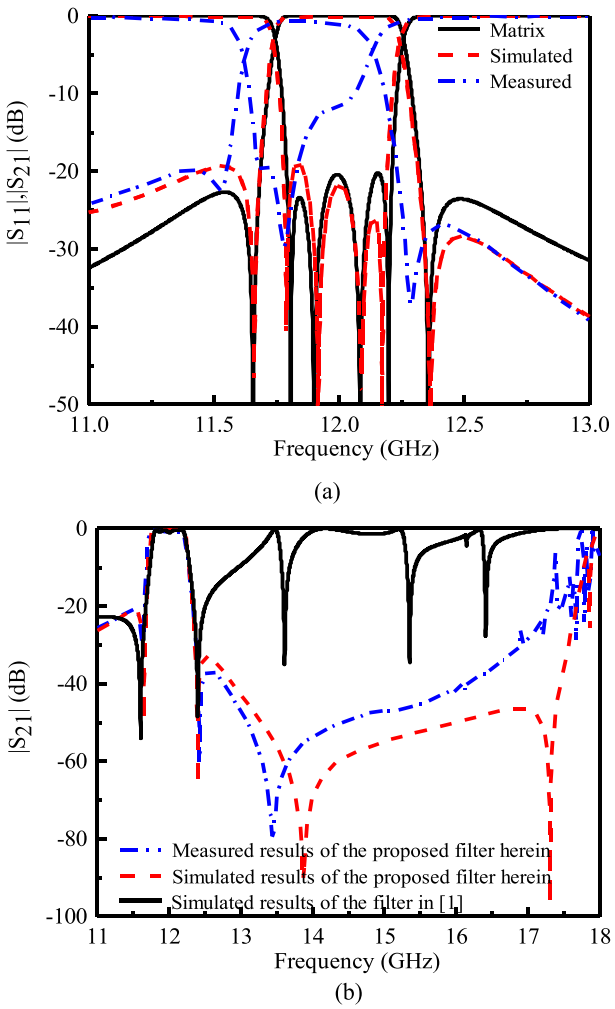

FIGURE 10. (a) Matrix, simulated and measured results of the in-band performance of the proposed fourth-order BPF; (b) Comparison of the out-of-band performance between the proposed filter and the filter in reference [1].

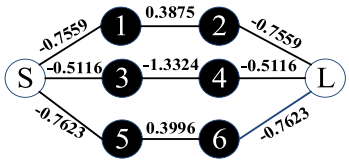

FIGURE 11. Topology of the proposed sixth-order BPF.

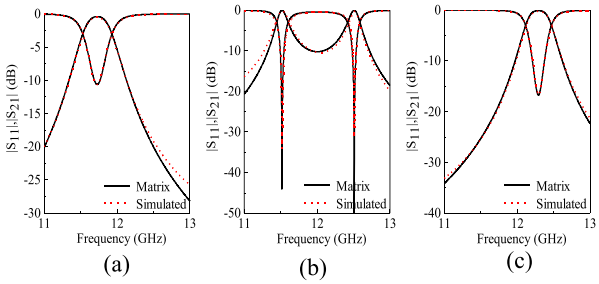

FIGURE 12. Comparison between simulated results and matrix of each sub-filter of the sixth-order BPF, (a) sub-filter 1, (b) sub-filter 2, (c) sub-filter 3.

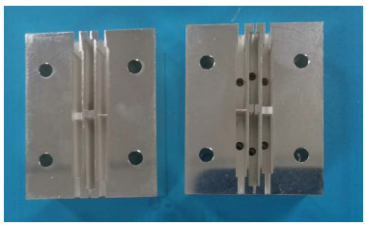

FIGURE 13. Photograph of the fabricated sixth-order BPF.

and 0.65 dB, respectively. The above discrepancies regard to center frequency and insertion loss are mainly attributed to the fabrication tolerances. In the fabricated filter, a_1, l_{12}, w_{11}, and w_{22}, which are critical and sensitive to the filtering response, are measured, and their measured values are 18.59, 7.63, 0.97, and 0.23 mm, respectively. The maximum deviation is about 70 μm, which mainly causes the discrepancies regard to the center frequency and insertion loss.

For a better comparison, a fourth-order transversal filter is designed in the simulator by using the topology and method in [1]. The comparison of the out-of-band performance of the two filters is shown in Fig. 10(b). The in-band responses of the two filters are almost the same, whereas the frequencies of the first spurious mode are different. For the filter proposed in [1], the first higher-order mode occurs at 13.47 GHz, which is 1.12 times the center frequency. For the filter proposed in this paper, the first higher-order mode occurs at 17.8 GHz, which is 1.48 times the center frequency. Obviously, the stopband has been well improved by using the proposed configuration herein.

In addition, a comparison with the reported waveguide BPFs is conducted and the results are presented in Table 1. It could be seen that the proposed BPF could simultaneously achieve a good trade-off in terms of wide stopband, good selectivity and compact size for filter design while preserving the attractive property of modular design, when compared with other reported filters.

IV. EXTENSION TO HIGH-ORDER BPFS

To further verify the foregoing analysis, this section applies the above procedures to implement two BPFs of the same

TABLE 1. Comparisons With Some Reported Waveguide BPFs

Ref.	CF (GHz)	SF (GHz)	Ratio (SF/CF)	Order	NO. of TZs	*IL* (dB)	Size ($\lambda_g/2\times\lambda_g/2\times\lambda_g/2$)
[1]	3.8	4.30	1.13	3	1	-	1*2*0.5
[2]	3.0	3.65	1.22	4	2	0.5	1*2*0.5
[3]	10.0	14.20	1.42	6	0	0.6	1*6*0.5
[6]	10.0	16.46	1.65	6	0	-	1*6*0.5
[7]	11.0	16.20	1.47	4	0	-	1*4*0.5
	11.0	16.30	1.48	8	0		1*8*0.5
[11]	22.7	44.10	1.94	6	0	0.5	2*3*0.5
[12]	9.5	13.80	1.45	5	0	-	1*5*0.5
[15]	11.0	16.1	1.46	8	0	-	1*8*0.5
[17]	4.5	6.5	1.44	4	2	-	1*4*0.5
This work	**12.0**	**17.80**	**1.48**	**4**	**2**	**0.65**	**1*2*0.5**

CF: center frequency; SF: frequency of the first spurious mode; λ_g: guided wavelength at the center frequency

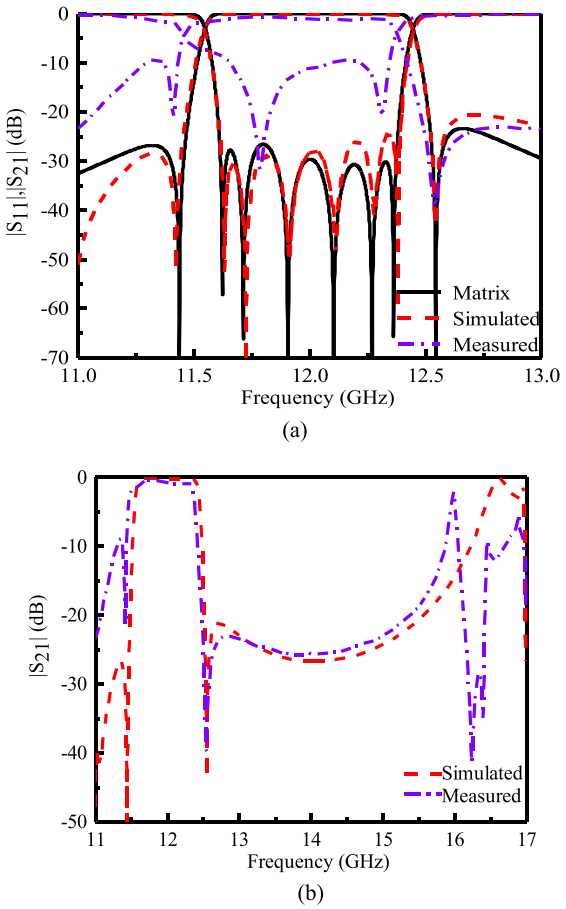

FIGURE 14. (a) Matrix, simulated and measured results of the in-band performance of the proposed sixth-order BPF; (b) The simulated and measured out-of-band performance of the proposed filter.

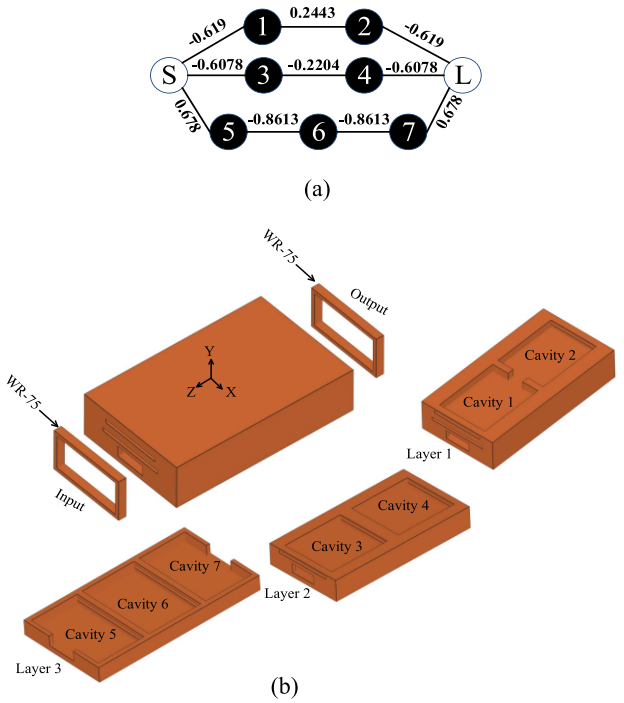

FIGURE 15. (a) Topology of the proposed seventh-order BPF; (b) Configuration of the proposed seventh-order BPF.

categories with higher order. Since the specific procedures have been described above, only the result of each case is given for brevity.

A. A SIXTH-ORDER BPF

The specification of the sixth-order BPF is as follows: working frequency $f_0 = 12$ GHz, bandwidth $BW = 800$ MHz, in-band return loss RL $\geq$ 20 dB, and two TZs are set at 11.4 GHz and 12.55 GHz, respectively. To achieve the specification, the topology in Fig. 11 is applied.

This topology could be implemented by adding another layer to the previous configuration. Due to the parallel coupling path, the filter could be divided into three sub-filters, and the comparison between the simulated and matrix of each sub-filter is shown in Fig. 12. The final values of all parameters are: $a_1 = 18.47$ mm, $a_2 = 18.4$ mm, $a_3 = 17.33$ mm, $b_1 = 3$ mm, $b_2 = 3$ mm, $b_3 = 3$ mm, $c_1 = 18.9$ mm, $c_2 = 20.5$ mm, $c_3 = 17$ mm, $h_{11} = 5$ mm, $h_{21} = 2.5$ mm, $h_{31} = 6$ mm, $h_{12} = 0.2$ mm, $h_{22} = 2$ mm, $h_{32} = 2$ mm, $l_{11} = 18.47$ mm, $l_{12} = 5.47$ mm, $l_{21} = 18.4$ mm, $l_{22} = 18.4$ mm, $l_{31} = 17.33$ mm, $l_{32} = 6.32$ mm, $s_1 = 0.3$ mm, $s_2 = 0.3$ mm, $w_{11} = 1.93$ mm, $w_{12} = 3$ mm, $w_{21} = 0.77$ mm, $w_{22} =$

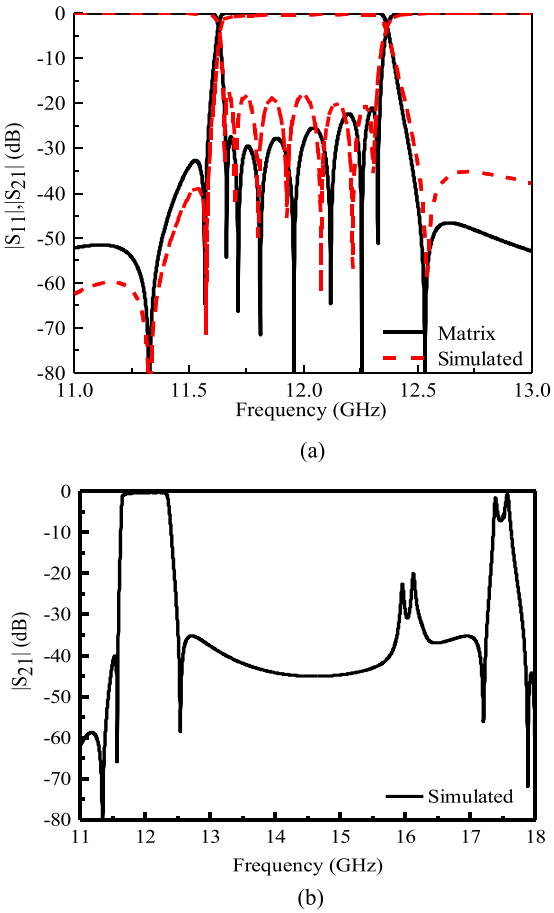

FIGURE 16. **(a) Matrix and simulated results of the in-band performance of the proposed seventh-order BPF; (b) The simulated out-of-band performance of the proposed filter.**

0.534 mm, $w_{31} = 1.6$ mm, $w_{32} = 3$ mm. s_1 is the distance between Layer 1 and Layer 2, and s_2 is the distance between Layer 2 and Layer 3. Similarly, the sixth-order filter is manufactured as shown in Fig. 13. The filtering response is shown in Fig. 14. It can be seen the simulated results in passband agree well with the matrix in terms of operating frequency and bandwidth. The first higher-order mode occurs at 16.6 GHz, which is 1.38 times the center frequency. Two TZs are generated out of the passband, leading to a very high selectivity. As for the measured results, the bandwidth of the passband and the position of the TZs are as expected, but the matching in the band is poor. In terms of insertion loss, the simulated and measured results are approximately 0.15 dB and 0.60 dB, respectively. The higher order mode measured occurs at 16.0 GHz, which is close to the expectation. In order to investigate the discrepancies between the simulated and measured results, a_1, w_{11}, w_{21}, w_{22}, a_3 and l_{32} are measured due to their high sensitivity to the filtering response, and their measured values are 18.54, 1.89, 0.72, 0.56, 17.3 and 6.26 mm, respectively. Their deviations to the nominal value are 0.07, 0.04, 0.05, 0.026, 0.03 and 0.06 mm, which are main causes of the poor return loss in the passband.

B. A SEVENTH-ORDER BPF

The specification of the seventh-order BPF is as follows: working frequency $f_0 = 12$ GHz, bandwidth BW = 680 MHz, in-band return loss RL $\geq$ 20 dB, and three TZs are set at 11.33 GHz, 11.57 GHz and 12.55 GHz, respectively. The topology is shown in Fig. 15(a).

The corresponding configuration is shown in Fig. 15(b). It can be seen there are three layers, and there are three cavities in the Layer 3 while two cavities in the other layers. The final values of all parameters are: $a_1 = 17.84$ mm, $a_2 = 18.92$ mm, $a_3 = 28.25$ mm, $b_1 = 2.9$ mm, $b_2 = 2.9$ mm, $b_3 = 3$ mm, $c_1 = 17$ mm, $c_2 = 20$ mm, $c_3 = 12.81$ mm, $c_4 = 14.38$ mm, $h_{11} = 5$ mm, $h_{21} = 1$ mm, $h_{31} = 1$ mm, $h_{12} = 4$ mm, $h_{22} = 6$ mm, $h_{32} = 3$ mm, $l_{11} = 17.84$ mm, l_{12}=7.26 mm, $l_{21} = 18.92$ mm, $l_{22} = 18.92$ mm, $l_{31} = 8.65$ mm, $l_{32} = 28.25$ mm, $s_1 = 0.3$ mm, s_2=0.3 mm, $w_{11} = 1.24$ mm, $w_{12} = 2.9$ mm, $w_{21} = 0.42$ mm, $w_{22} = 0.096$ mm, $w_{31} = 3$ mm, $w_{32} = 0.198$ mm. c_3 is the length of the cavity on both sides of the Layer 3, and c_4 is the length of the cavity in the center of the Layer 3. The filtering response of the seventh-order BPF is shown in Fig. 16. It could be seen that the simulated results well accord with filtering response of the coupling matrix. The first higher order mode occurs at 17.4 GHz, which is 1.45 times the center frequency.

V. CONCLUSION

In this paper, a class of waveguide BPFs with parallel coupling topology are modularly designed by stacking cascaded rectangular cavities, instead of one cavity. Due to the parallel coupling topology, each layer could realize a sub-filter independently. The stopband of filter could be widened by properly setting the width-length ratio of rectangular cavities. A fourth-order BPF is designed in detail to illustrate the design process. Besides, two additional higher-order BPFs are designed by applying the process. Among them, the fourth-order BPF are fabricated and measured. These measured and simulated results well verify the improvement of stopband and the validity of the proposed approaches. Additionally, the produced TZs makes this class of filters possess high selectivity.

REFERENCES

[1] Z.-C. Guo, L. Zhu, and S.-W. Wong, "Synthesis of transversal bandpass filters on stacked rectangular H-plane waveguide cavities," *IEEE Trans. Microw. Theory Techn.*, vol. 67, no. 9, pp. 3651–3660, Sep. 2019.

[2] Z.-C. Guo, L. Zhu, and S.-W. Wong, "Modular synthesis of waveguide bandpass filters using dual-mode resonators," *IEEE Trans. Microw. Theory Techn.*, vol. 68, no. 5, pp. 1660–1667, May 2020.

[3] M. Morelli, I. Hunter, R. Parry, and V. Postoyalko, "Stopband performance improvement of rectangular waveguide filters using stepped-impedance resonators," *IEEE Trans. Microw. Theory Techn.*, vol. 50, no. 7, pp. 1657–1664, Jul. 2002.

[4] R. J. Cameron, M. Yu, and Y. Wang, "Direct-coupled microwave filters with single and dual stopbands," *IEEE Trans. Microw. Theory Techn.*, vol. 53, no. 11, pp. 3288–3297, Nov. 2005.

[5] Y. Su, Y. Fan, X. Q. Lin, and K. Wu, "Single-layer mode composite coplanar waveguide dual-band filter with large frequency ratio," *IEEE Trans. Microw. Theory Techn.*, vol. 68, no. 6, pp. 2320–2330, Jun. 2020.

[6] M. Morelli, I. Hunter, R. Parry, and V. Postoyalko, "Stop-band improvement of rectangular waveguide filters using different width resonators: Selection of resonator widths," in *IEEE MTT-S Int. Microw. Symp. Dig.*, 2001, pp. 1623–1626.
[7] J. Valencia, V. E. Boria, M. Guglielmi, and S. Cogollos, "Compact wideband hybrid filters in rectangular waveguide with enhanced out-of-band response," *IEEE Trans. Microw. Theory Techn.*, vol. 68, no. 1, pp. 87–101, Jan. 2020.
[8] S.-C. Lin, P.-H. Deng, Y.-S. Lin, C.-H. Wang, and C.H. Chen, "Wide-stopband microstrip bandpass filters using dissimilar quarter-wavelength stepped-impedance resonators," *IEEE Trans. Microw. Theory Techn.*, vol. 54, no. 3, pp. 1011–1018, Mar. 2006.
[9] J.-T. Kuo and E. Shih, "Microstrip stepped impedance resonator bandpass filter with an extended optimal rejection bandwidth," *IEEE Trans. Microw. Theory Techn.*, vol. 51, no. 5, pp. 1554–1559, May 2003.
[10] P. Zhao, X. Wang, and C. Chen, "Rectangular waveguide band-pass filter with high power harmonic suppression," in *Proc. 15th Int. Conf. Electron. Packag. Technol.*, 2014, pp. 1327–1328.
[11] Q. Wu, F. Zhu, Y. Yang, and X. Shi, "An effective approach to suppressing the spurious mode in rectangular waveguide filters," *IEEE Microw. Wireless Compon. Lett.*, vol. 29, no. 11, pp. 703–705, Nov. 2019.
[12] D. Budimir, "Optimized E-plane bandpass filters with improved stopband performance," *IEEE Trans. Microw. Theory Techn.*, vol. 45, no. 2, pp. 212–220, Feb. 1997.
[13] R. Vahldieck and W. J. R. Hoefer, "Finline and metal insert filters with improved passband separation and increased stopband attenuation," *IEEE Trans. Microw. Theory Techn.*, vol. 33, no. 12, pp. 1333–1339, Dec. 1985.
[14] A. Iqbal, A. W. Ahmad, A. Smida, and N. K. Mallat, "Tunable SIW bandpass filters with improved upper stopband performance," *IEEE Trans. Circuits Syst. II, Exp. Briefs*, vol. 67, no. 7, pp. 1194–1198, Jul. 2020.
[15] A. Iqbal, J. J. Tiang, S. K. Wong, S. W. Wong, and N. K. Mallat, "QMSIW-Based single and triple band bandpass filters," *IEEE Trans. Circuits Syst. II, Exp. Briefs*, vol. 68, no. 7, pp. 2443–2447, Jul. 2021.
[16] L. Chen, Z.-C. Guo, and G. Zhang, "Modular design of a fourth-order waveguide bandpass filter with high selectivity," in *Proc. Cross Strait Radio Sci. Wireless Technol. Conf.*, 2021, pp. 348–350.
[17] J.-S. Hong and M. Lancaster, *Microstrip Filters for RF/Microwave Applications*. New York, NY, USA: Wiley, 2001.
[18] J. Valencia, M. Guglielmi, S. Cogollos, J. Vague, and V. E. Boria, "Enhancing the performance of stepped impedance resonator filters in rectangular waveguide," in *Proc. 47th Eur. Microw. Conf.*, 2017, pp. 989–992.
[19] S. Li, J. Fu, and X. Wu, "Analysis of high-power rectangular waveguide filter with capacitive coupling iris for satellite," in *Proc. Asia–Pacific Power Energy Eng. Conf.*, 2009, pp. 1–4.
[20] J. A. Ruiz-Cruz, K. A. Zaki, J. R. Montejo-Garai, and J. M. Rebollar, "Rectangular waveguide elliptic filters with capacitive and inductive irises and integrated coaxial excitation," in *IEEE MTT-S Int. Microw. Symp. Dig.*, 2005, pp. 269–272.

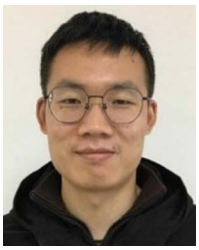

ZAI-CHENG GUO received the B.Eng. and M.Eng. degrees in electronic engineering from the South China University of Technology, Guangzhou, China, in 2013, and 2016, respectively, and the Ph.D. degree in electrical and computer engineering from the University of Macau, Macau, China, in 2020. From February 2016 to May 2016, he joined the Southern University of Science and Technology, Shenzhen, China, as an Exchange Student. In 2020, he joined the School of Electrical and Automation Engineering, Nanjing Normal University, Nanjing, China, as an Assistant Professor. His research interests include microwave passive component design and optimization.

LONGJI CHEN was born in Jiangsu, China, in 1997. He received the B.S. degree from the School of Electrical Engineering, Jiangsu University, Zhenjiang, China, in 2020. He is currently working toward the M.S. degree in electrical and automation engineering with Nanjing Normal University, Jiangsu, China. His research interests include design and optimization of microwave filters.

LEI ZHU (Fellow, IEEE) received the B.Eng. and M.Eng. degrees in radio engineering from the Nanjing Institute of Technology (now Southeast University), Nanjing, China, in 1985 and 1988, respectively, and the Ph.D. degree in electronic engineering from the University of Electro-Communications, Tokyo, Japan, in 1993.

From 1993 to 1996, he was a Research Engineer with Matsushita-Kotobuki Electronics Industries Ltd., Tokyo, Japan. From 1996 to 2000, he was a Research Fellow with the École Polytechnique de Montréal, Montréal, QC, Canada. From 2000 to 2013, he was an Associate Professor with the School of Electrical and Electronic Engineering, Nanyang Technological University, Singapore. He joined the Faculty of Science and Technology, University of Macau, Macau, China, as a Full Professor in August 2013, and has been a Distinguished Professor since December 2016. From August 2014 to August 2017, he was the Head of Department of Electrical and Computer Engineering, University of Macau. He has authored or coauthored more than 700 papers in international journals and conference proceedings. His papers have been cited more than 12500 times with the H-index of 55 (source: Scopus). His research interests include microwave circuits, antennas, periodic structures, and computational electromagnetics.

Dr. Zhu was an Associate Editor of the IEEE TRANSACTIONS ON MICROWAVE THEORY AND TECHNIQUES (2010–2013) and IEEE MICROWAVE AND WIRELESS COMPONENTS LETTERS (2006–2012). He was the General Chair of the 2008 IEEE MTT-S International Microwave Workshop Series on the Art of Miniaturizing RF and Microwave Passive Components, Chengdu, China, and Technical Program Committee Co-Chair of the 2009 Asia–Pacific Microwave Conference, Singapore. He was a member of IEEE MTT-S Fellow Evaluation Committee (2013–2015) and a member of IEEE AP-S Fellows Committee (2015–2017). He was the recipient of the 1997 Asia–Pacific Microwave Prize Award, the 1996 Silver Award of Excellent Invention from Matsushita-Kotobuki Electronics Industries Ltd., the 1993 Achievement Award in Science and Technology (first prize) from the National Education Committee of China, the 2020 FST Research Excellence Award from the University of Macau, and the 2020 Macao Natural Science Award (second prize) from the Science and Technology Development Fund (FDCT), Macau, China.